

Spin Fluctuations in the Underdoped High- T_c Cuprate $\text{La}_{1.93}\text{Sr}_{0.07}\text{CuO}_4$

H. HIRAKA, Y. ENDOH

Institute for Materials Research, Tohoku University, Sendai 980-8577

M. FUJITA

The Institute for Chemical Research, Kyoto University, Uji 611-0011

Y. S. LEE

National Institute of Standards and Technology, NIST center for Neutron Research, Gaithersburg, Maryland 20899, U.S.A.

J. KULDA, A. IVANOV

Institut Laue-Langevin, 156X, 38042 Grenoble Cedex 9, France

R. J. BIRGENEAU

Department of Physics, University of Toronto, Toronto M5S 1A1, Canada

(November 2, 2018)

We performed magnetic inelastic neutron-scattering experiments on $\text{La}_{1.93}\text{Sr}_{0.07}\text{CuO}_4$ over a wide range of ω and T ; $2 \leq \omega \leq 44$ meV and $1.5 \leq T < 300$ K. The dynamic susceptibility $\chi''(\mathbf{q}, \omega)$ of this underdoped high- T_c superconductor ($T_c = 17$ K) is characterized by broad, incommensurate peaks. Here, the incommensurate wavevector δ_ω is approximately 0.07 reciprocal lattice units at low T and ω . The superconducting phase does not possess an observable gap in the spin excitation spectrum down to at least 2 meV. Scaling behavior is demonstrated for the Q -integrated energy spectrum $\chi''(\omega)_T$ with respect to $(\omega/k_B T)$. This scaling establishes a connection between the magnetic excitations of the compositions on either side of the insulator-superconductor boundary in the $\text{La}_{2-x}\text{Sr}_x\text{CuO}_4$ phase diagram. We note a possible cross-over from an incommensurate to a commensurate response for $\omega > 20$ meV or $T > 300$ K.

PACS numbers:

I. INTRODUCTION

Magnetic inelastic neutron-scattering (INS) experiments have been performed to investigate the relationship between high- T_c superconductivity,^{1,2} and the strong two-dimensional (2D) spin fluctuations of the CuO_2 plane. It is well known that inelastic magnetic peaks appear at incommensurate positions in momentum space for $\text{La}_{2-x}\text{Sr}_x\text{CuO}_4$ (LSCO) superconductors. Recently, Yamada *et al.* systematically studied the low-energy magnetic excitations by using crucible-free high-quality single crystals.³ They found a direct proportionality between the hole concentration (x), dynamic incommensurability (δ_ω), and T_c for the underdoped superconductors. There is also a clear gap in the low-energy spin excitations for optimally doped $\text{La}_{1.85}\text{Sr}_{0.15}\text{CuO}_4$ and slightly over-doped $\text{La}_{1.82}\text{Sr}_{0.18}\text{CuO}_4$.^{4,5} These latter compounds do not possess static magnetic order.

Recent elastic neutron-scattering experiments revealed that incommensurate static magnetic correlations exist in the CuO_2 planes for both the spin-glass insulators⁶⁻⁸ and the underdoped superconductors^{9,10}. A remarkable feature is that the positions of the incommensurate peaks change dramatically as a function of hole concentration at the insulator-to-superconductor boundary of $x_{\text{cr}} \simeq 0.055$.⁸ That is, the incommensurate wavevector is approximately parallel to the Cu-O-Cu direction in the

superconductors, but is at 45° to this direction in the insulators. At the special doping level of $x = 0.12$, the incommensurate peaks are resolution-limited, indicating that the spins are correlated over distances exceeding 200 Å within the CuO_2 plane, and the peaks appear below T_c .^{9,11} For the materials with static order, the inelastic scattering peaks occur at the same positions as those of the elastic peaks within error.

Neutron experiments with high transferred energies have focused primarily on antiferromagnetic LCO^{12,13} and optimally doped LSCO^{14,15}. To-date, few detailed studies of the high-energy spin fluctuations have been reported for LSCO superconductors near the insulator-superconductor boundary of the phase diagram. The non-superconducting spin-glass compositions have been carefully studied by Keimer *et al.*¹⁶ and Matsuda *et al.*¹⁷ for $\text{La}_{1.96}\text{Sr}_{0.04}\text{CuO}_4$ and $\text{La}_{1.98}\text{Sr}_{0.02}\text{CuO}_4$, respectively. They observed commensurate spin fluctuations for $\omega > 3$ meV and demonstrated scaling behavior of $\chi''(\omega)$ with respect to the variable $(\omega/k_B T)$ over a wide range of T and ω .

We have performed a systematic study of the spin fluctuations in $\text{La}_{1.93}\text{Sr}_{0.07}\text{CuO}_4$ to explore the behavior of $\chi''(\mathbf{q}, \omega)$ in a system with hole concentration slightly above x_{cr} . We find that the magnetic-excitation spectrum is gapless. Also, the ω and T dependences indicate scaling behavior similar to that in the lightly-

doped spin-glass compositions. There is possibly an incommensurate-to-commensurate transition at high energy transfers or high temperatures. This paper is organized as follows. Section 2 describes the experimental procedures and results. A discussion of the data is given in § 3, and § 4 contains the conclusion.

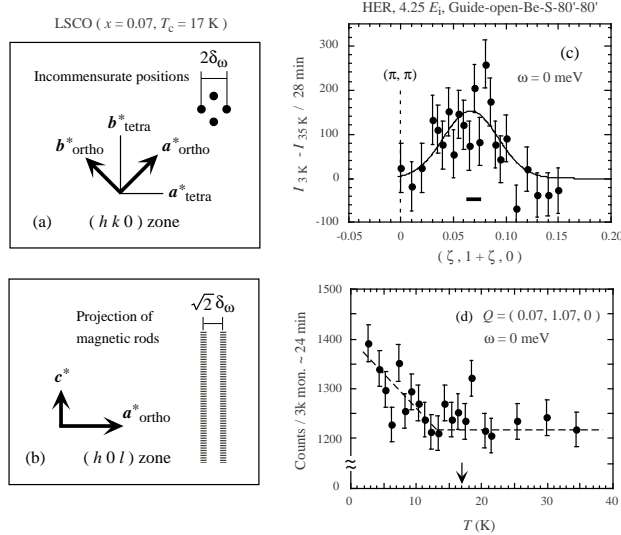


Fig.1 / H. Hiraka *et al.*

FIG. 1. (a) and (b): Scattering geometries in the $(hk0)$ and $(h0l)$ zones, respectively. A magnetic four-rod structure is presented (a) as the cross section giving four incommensurate points on the tetragonal axes, and (b) as the projection onto the $(a^*_{\text{ortho}} - c^*)$ plane with two parallel lines hatched along c^* . (c) and (d): Elastic scattering in the (a)-type geometry. (c) An incommensurate peak in a difference plot between 3 K and 35 K. The horizontal short bar represents the instrumental resolution. (d) Thermal evolution of the peak intensity. The arrow labels T_c . The broken line is a guide to the eye.

II. EXPERIMENTAL PROCEDURE AND RESULTS

The travelling-solvent-floating-zone method was utilized for the single-crystal growth as described previously.^{18,7} The onset T_c of 17 K was determined from dc-susceptibility measurements and agrees with the linear relation between T_c and δ_ω .³ INS experiments were carried out on the triple-axis spectrometers (TOPAN, IN8, IN20 and IN22) installed at thermal-neutron beam ports of the JRR-3M in JAERI and of the high-flux reactor in ILL. Either a pyrolytic-graphite (PG) monochromator or a copper monochromator was used to monochromatize

the incident neutrons. A PG analyzer was used to select neutrons scattered from the sample. In most cases, a PG filter was placed in front of the analyzer to remove higher-order neutrons from the scattered beam. However, at IN20, we used a silicon analyzer utilizing the (111) reflection without a filter. The sample (7 mm $\phi \times 30$ mm) was set up in a He^4 closed-cycle refrigerator or a pumped He^4 cryostat with He exchange gas. A twin structure exists in the low-temperature orthorhombic phase, in which two domains are distributed with nearly equal populations. The orthorhombicity of $(b_{\text{ortho}}/a_{\text{ortho}})$ in $Bmab$ notation is 1.005 at 1.5 K. Figures 1(a) and 1(b) show the scattering geometries in the $(hk0)$ and $(h0l)$ zones, respectively. We conducted \mathbf{q} scans along $\mathbf{q}_{2D} = [h, \pm h, 0]$ and $[h, 0, 0]$ for each configuration, in order to pass through a pair of incommensurate peaks.

The scattering function $S(\mathbf{q}, \omega)$ is directly connected to $\chi''(\mathbf{q}, \omega)$ via the relation $S(\mathbf{q}, \omega) = (n + 1)\chi''(\mathbf{q}, \omega)$ where $n = (\exp(\hbar\omega/k_B T) - 1)^{-1}$. We model the magnetic cross-section as four rods running along c^* in reciprocal space as illustrated in Figs. 1(a) and 1(b).^{20,21} $\chi''(\mathbf{q}_{2D}, \omega)$ is parameterized by four squared Lorentzians; $\chi''(\mathbf{q}_{2D}, \omega) = \chi''(\omega) \sum_{n=1}^4 K_\omega^2 / [(\mathbf{q}_{2D} - \delta_n(\omega))^2 + K_\omega^2]^2$. Here, $\delta_n(\omega)$ denotes the incommensurate wavevector and K_ω denotes the q -width in the $(a^*_{\text{ortho}} - b^*_{\text{ortho}})$ plane. $\chi''(\omega)_T$ is proportional to the \mathbf{q} integration of $\chi''(\mathbf{q}, \omega)$ over the entire Brillouin zone, and the suffix T emphasizes the temperature variation. Instrumental resolution effects²² were convolved with the above cross-section.

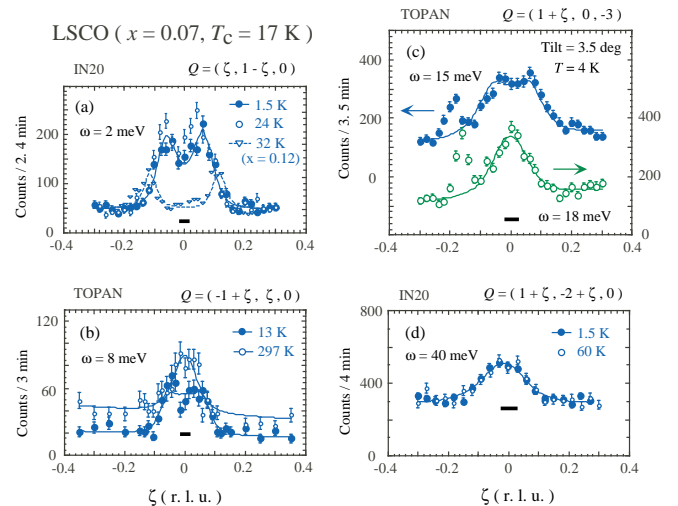


Fig. 2 / H. Hiraka *et al.*

FIG. 2. (a)-(d): \mathbf{q}_{2D} spectra at various ω and T . Instrumental energies and collimations are as follows: (a) $14.7 E_f$, Open-40'-40'-Open, (b) $14.7 E_f$, Open-30'-30'-Open, (c) $13.5 E_f$, Open-60'-60'-Open and (d) $18.7 E_f$, Open-40'-40'-Open. The solid lines show the fitting results with resolution effects convoluted, under a restriction in the peak width. The horizontal short bars represent the relevant instrumental q resolutions. As a reference, an incommensurate peak structure observed in $\text{La}_{1.88}\text{Sr}_{0.12}\text{CuO}_4$ ($T_c = 31$ K) is also depicted in (a) after normalization with the sample volume and monitor time. The broken line is a guide to the eye.

Before a detailed description of inelastic scattering measurements, we briefly comment on the static correlations observed in this sample. Elastic neutron scattering was measured with the triple-axis spectrometer (HER) placed in the cold-neutron beam line of JAERI. At low T , magnetic elastic peaks appear at incommensurate positions with $\delta_0 \simeq 0.069a_{\text{tetra}}^*$. As shown in Fig. 1(c), the static response is weak and broad in momentum space ($\kappa_0^{7\%} = 0.037 \text{ \AA}^{-1}$), compared to the resolution-limited peaks in $\text{La}_{1.88}\text{Sr}_{0.12}\text{CuO}_4$ ($\kappa_0^{12\%} \leq 0.005 \text{ \AA}^{-1}$).⁹ The short-range static correlation length ($1/\kappa_0^{7\%} \leq 30 \text{ \AA}$) and the small ordered moment are consistent with the general trend found for superconducting compositions with $x < 0.12$.⁹ The elastic scattering merges into the background level above ~ 12 K, slightly lower than T_c as demonstrated in Fig. 1(d). The detailed results and analyses of the elastic component will be reported elsewhere.⁸

We display representative scans through the rods of magnetic scattering for various energy transfers and temperatures in Figs. 2(a)-2(d). At low ω and T , the inelastic scattering is incommensurate with peaks at the same positions as those seen in the elastic channel. Pronounced scattering survives even down to 2 meV at 1.5 K as shown in Fig. 2(a). Therefore, in this compound any magnetic gap in the superconducting state must be at energies much less than 2 meV. At higher energy transfers and temperature, we see evidence for a possible crossover from a double to a single peak structure in the raw \mathbf{q}_{2D} profiles shown in Figs. 2(b) and 2(c). Unfortunately, phonon scattering severely contaminates the \mathbf{q}_{2D} profiles in the medium-energy range of $12 < \omega < 30$ meV, as seen at $\zeta \approx -0.2$ r.l.u. in Fig. 2(c). Hence, the precise evolution of the line-shapes from the low energy to the high energy regime is difficult to obtain. The temperature evolution of the magnetic scattering for $\omega = 4$ meV is depicted in Fig. 3. The peak intensity and the incommensurate splitting both appear to decrease gradually with increasing T .

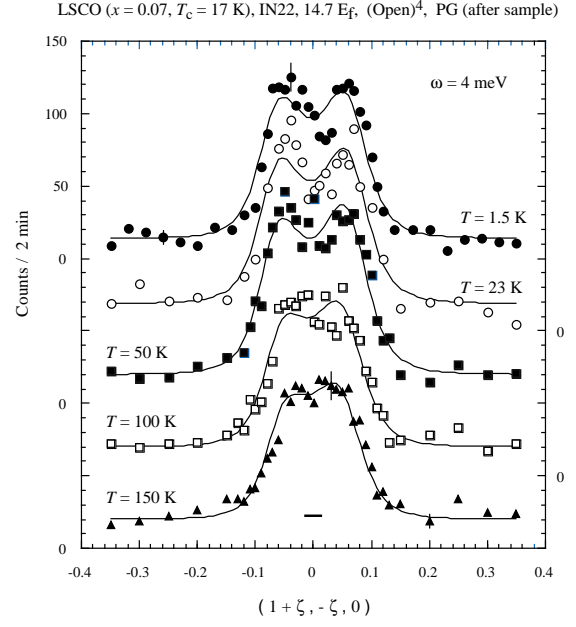


Fig. 3 / H. Hiraka *et al.*
FIG. 3. Temperature variation of low-energy incommensurate peaks with $\omega = 4$ meV. The solid lines show the results of resolution-convoluted fits by using the same condition for the peak widths, as the fits depicted in Figs. 2(a) - 2(d). The horizontal short bar represents the instrumental q resolution.

For the initial data analysis, we allowed the parameters δ_ω , K_ω , $\chi''(\omega)$ and a sloped background along \mathbf{q}_{2D} to vary independently. However, in the high- ω or high- T region, the fits do not converge uniquely; a large K_ω or a small δ_ω can be invoked to describe the data. In order to be systematic and obtain physically consistent fits, we assumed a smooth increase in $K_{\omega,T}$ with increasing ω and temperature: $(K_{\omega,T})^2 = (K_{0,0})^2 + a_0^{-2}[(k_B T/E_T)^2 + (\omega/E_\omega)^2]$ with $K_{0,0} = 0.065 \text{ \AA}^{-1}$, $a_0 = 3.79 \text{ \AA}$ and $E_T = E_\omega = 85$ meV. This form was used by Aeppli *et al.*²³ to explain the peak widths observed in $\text{La}_{1.86}\text{Sr}_{0.14}\text{CuO}_4$. The above expression for $\text{La}_{1.93}\text{Sr}_{0.07}\text{CuO}_4$ describes the overall behavior of $K_{\omega,T}$ fairly well. The fits to the \mathbf{q}_{2D} spectra are shown in Figs. 2(a) - 2(d) and 3. $K_{0,0}$ corresponds to $\kappa_{0,0}^{7\%} = 0.042 \text{ \AA}^{-1}$. The extrapolated value is compatible with the value obtained for $\kappa_0^{7\%}$ from the elastic scattering, but it is about twice as large as $\kappa_{0,0}^{14\%} = 0.022 \text{ \AA}^{-1}$ ²³ and $\kappa_{\omega,T}^{4\%, 2.4\%} \sim 0.02 \text{ \AA}^{-1}$ found at low ω and low T .^{16,7} As a further comparison, Fig. 2(a) also displays the sharp incommensurate peaks observed in $\text{La}_{1.88}\text{Sr}_{0.12}\text{CuO}_4$ ($T_c = 31$ K), which are much narrower than those we find in $\text{La}_{1.93}\text{Sr}_{0.07}\text{CuO}_4$.

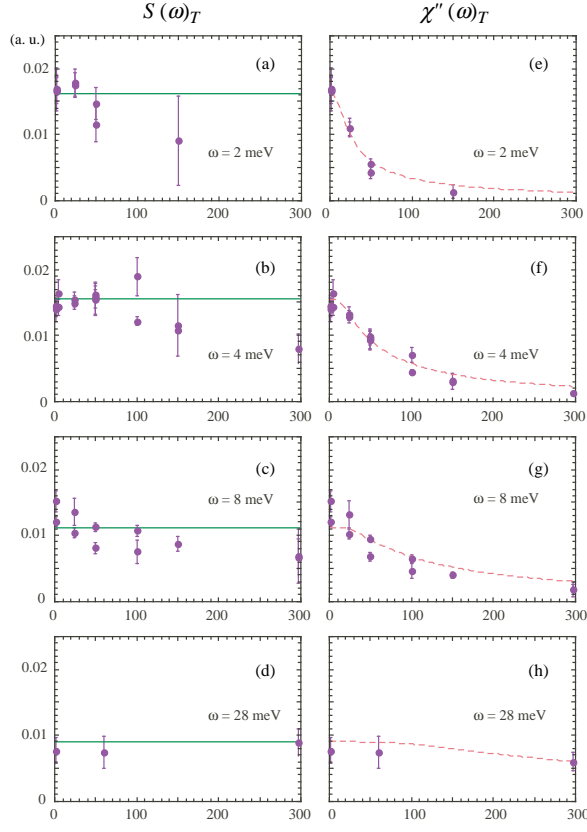


FIG. 4. Temperature dependence of $S(\omega)_T$ in (a)-(d) and of $\chi''(\omega)_T$ in (e)-(h). The solid straight lines in (a)-(d) are drawn, assuming that $S(\omega)_T$ is constant as a function of T , while the broken curves in (e)-(h) are calculated assuming $\chi''(\omega)_T = \chi''(\omega)_{1.5\text{K}} / (n(\omega, T) + 1)$.

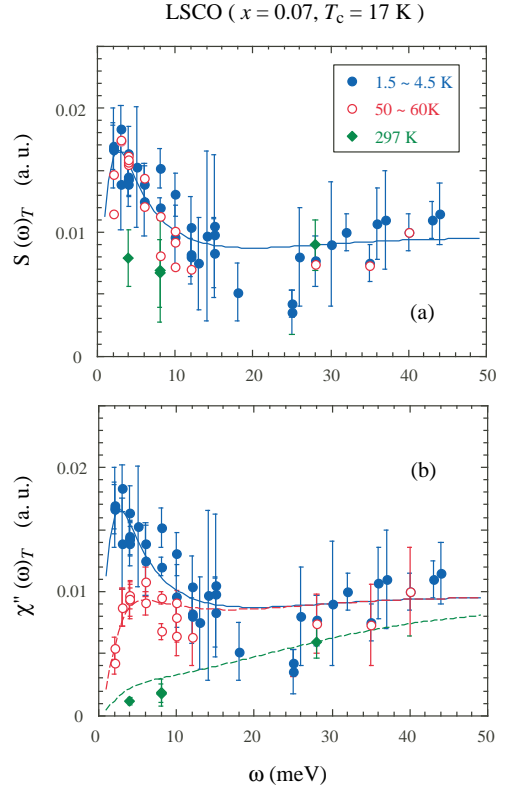


FIG. 5. ω dependence of (a) $S(\omega)_T$ and (b) $\chi''(\omega)_T$. The solid line for $\chi''(\omega)_{1.5\text{K}}$ represents the addition of two putative damped Lorentzians; $\omega \sum_{n=L,H} c_n \Gamma_n / (\omega^2 + \Gamma_n^2)$, where the characteristic energies Γ_L and Γ_H were arbitrarily chosen to be 2.5 and 60 meV, respectively, with the ratio of coefficients c_L/c_H of 2. The broken lines in (b) show the thermal evolution calculated by $\chi''(\omega)_T = \chi''(\omega)_{1.5\text{K}} / (n(\omega, T) + 1)$.

The T dependences of $\chi''(\omega)_T$ and $S(\omega)_T$ are depicted in Figs. 4 and 5 for various values of ω . $S(\omega)_T$ is the \mathbf{q}_{2D} integration of $S(\mathbf{q}, \omega)$, and depends weakly on T . A remarkable feature of $\chi''(\omega)_T$ is that low-energy fluctuations grow significantly with decreasing T . This is in contrast to the complete gap seen in the excitation spectrum of the optimal superconductor. The data in Fig. 5 also indicate that the spectral weight in the high-energy range (> 20 meV) is nearly constant, or tends to increase slightly with increasing ω . We plot $\chi''(\omega)_T$ as a function of the scaled variable $(\omega/k_B T)$ in Fig. 6(a). The data with $\omega < 20$ meV (open circles) roughly show a maximum at $(\omega/k_B T) \sim 10$. This behavior is similar to that in $\text{YBa}_2\text{Cu}_3\text{O}_{6+x}$ (YBCO) with $x = 0.4$ located near the antiferromagnetic-superconducting phase boundary.²⁴ Higher-energy excitations (solid circles) are also shown. Figure 6(b) shows $\chi''(\omega)_T$ divided by an ω -dependent normalization factor measured at $T = 1.5$ K.^{16,17}

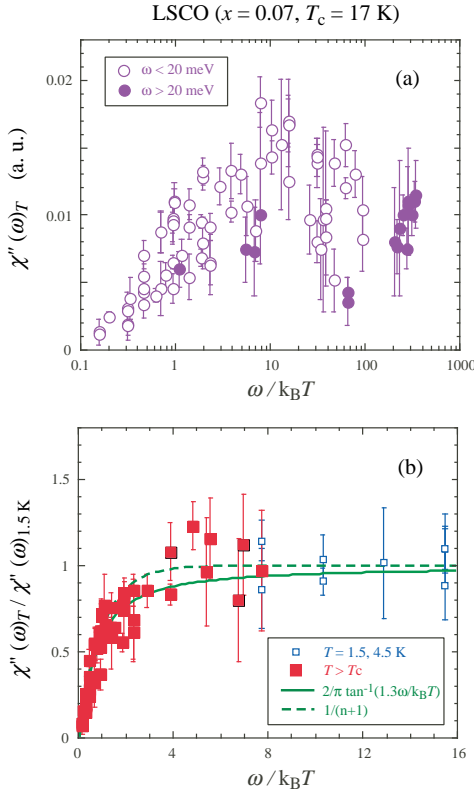


FIG. 6. (a) Direct replot of $\chi''(\omega)_T$ versus $(\omega/k_B T)$. Note that the horizontal axis is on a logarithm in scale. (b) Conventional scaling plot for small $(\omega/k_B T)$. The solid and broken lines represent $(2/\pi)\tan^{-1}(1.3(\omega/k_B T))$ and $(n(\omega, T) + 1)^{-1}$, respectively.

III. DISCUSSION

Our main result is the determination of the magnetic excitation spectrum of $\text{La}_{1.93}\text{Sr}_{0.07}\text{CuO}_4$ for $2 \leq \omega \leq 44$ meV for various temperatures. At low temperatures, the upturn of $\chi''(\omega)$ with decreasing energy transfer is similar to the behavior observed in the non-superconducting, spin-glass compositions.^{16,17} This indicates that the low-energy spin fluctuations retain their same basic character even as one crosses the insulator-superconductor boundary. We note, however, that the elastic scattering at the incommensurate positions in $\text{La}_{1.93}\text{Sr}_{0.07}\text{CuO}_4$ is weaker than the strong quasi-elastic scattering observed in $\text{La}_{1.96}\text{Sr}_{0.04}\text{CuO}_4$ and $\text{La}_{1.98}\text{Sr}_{0.02}\text{CuO}_4$. $S(\omega)_T$ is largely independent of temperature as seen in Fig. 4. This indicates that $(\chi''(\omega)_T / \chi''(\omega)_{1.5\text{ K}})$ has a T -dependence that roughly follows the inverse of the Bose thermal factor $(n(\omega, T) + 1)^{-1}$. The scaling function $\tan^{-1}(1.3\omega/k_B T)$ also explains the $(\omega/k_B T)$ dependence in Fig. 6(b) to within the errors. The latter scaling function has been used to describe the data for $\chi''(\omega)_T$ in $\text{La}_{1.96}\text{Sr}_{0.04}\text{CuO}_4$ and $\text{La}_{1.98}\text{Sr}_{0.02}\text{CuO}_4$ over a wide $(\omega \geq 3 \text{ meV}, T)$ regime.^{16,17}

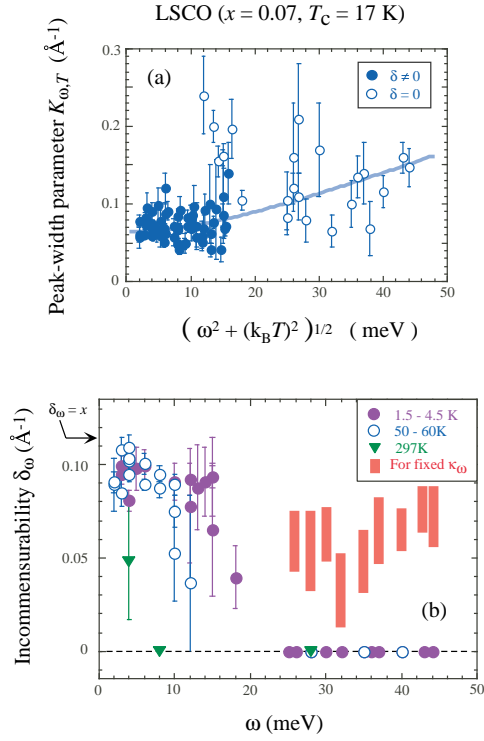


FIG. 7. (a) Peak-width parameter $K_{\omega,T}$ when no restriction is used in the \mathbf{q} -profile fits. A smooth increase of $K_{\omega,T}$ against ω and T (a curved line) is assumed in the main analysis. (b) Resolution-corrected incommensurability δ_ω . Based on the above assumption for $K_{\omega,T}$, a significant change of δ_ω is deduced. If the peak width is held constant ($\kappa_\omega = 0.04 \text{ r.l.u.} = 0.047 \text{ \AA}^{-1}$, $K_\omega = 0.073 \text{ \AA}^{-1}$), then δ_ω so-deduced remains non-zero up to the highest energy measured. (Vertical thick bars.)

Of particular interest is the energy scale of the dynamic incommensurate correlations. The scattering profiles evolve from a well-resolved, double-peaked structure at low temperatures and energies to a broad, single peaked structure with increasing ω and T . At this stage, we cannot say with certainty that an incommensurate-to-commensurate cross-over exists. However, a simple analysis of the data points in this direction. If we assume that $K_{\omega,T}$ evolves smoothly with T as shown in the top panel of Fig. 7, then the detailed fits revealed that δ_ω goes to zero at around $\omega_{7\%} = 20$ meV at low T as plotted in the lower panel. This energy scale of about 20 meV is reasonable in light of similar incommensurate-to-commensurate cross-over behavior seen in other LSCO compounds: $\omega_{2.4\%} = 7 \text{ meV}$ ⁷, $\omega_{10\%} \approx 25 \text{ meV}$ ²⁵, and $\omega_{15\%} > 50 \text{ meV}$.²⁶ In addition, the temperature dependence of $\chi''(\omega)_{1.5\text{ K}}$ changes slope across ω of 20 meV as shown in Fig. 5(b). With increasing temperature, δ_ω decreases and appears to go to zero at about 300 K ($\sim 25 \text{ meV}$ in energy units). This consistency between the crossover energy and temperature is also seen in $\text{La}_{1.976}\text{Sr}_{0.024}\text{CuO}_4$.⁷ Alternatively, the

incommensurability δ_ω may remain non-zero up to the highest measured energy transfers, if we assume a constant $\kappa_{\omega,T} = 0.04$ r.l.u. for the whole energy range. This restriction appears to be less likely, and the profiles shown in Figs. 2 and 3 are fit better if an incommensurate-to-commensurate cross-over does indeed occur.

In superconducting $\text{La}_{1.93}\text{Sr}_{0.07}\text{CuO}_4$, the observations of an enhancement of $\chi''(\omega)$ at low ω , the scaling function with a form of $\tan^{-1}(\omega/k_B T)$, and the incommensurate-to-commensurate crossover at a finite energy, are all reminiscent of the behavior observed in the non-superconducting spin-glass compositions.^{16,17,7} Even though the positions of the elastic incommensurate scattering changes dramatically as the doping level crosses the insulator-to-superconductor boundary,⁶ it appears that the behavior of the inelastic spin excitations evolves quite smoothly. This is consistent with the apparent observation of spin-glass ordering in the underdoped superconducting region observed by μSR measurements.^{27,28} Also, the saturation of κ_ω below 10 meV or 100 K in Fig. 7(a) is similar to the behavior of the inverse correlation lengths of spin-glass compounds.¹⁶

IV. CONCLUSION

We have conducted magnetic inelastic neutron scattering experiments on $\text{La}_{1.93}\text{Sr}_{0.07}\text{CuO}_4$ over a wide range of ω and T . The low-energy incommensurate fluctuations are enhanced at low T , with no indication of a magnetic gap in this underdoped superconductor. The dependence of $\chi''(\omega)$ on T and ω is observed to depend primarily on the scaled variable $(\omega/k_B T)$. By following the scattering profiles to high energy, we conjecture that an incommensurate-to-commensurate crossover occurs at $\omega \sim 20$ meV or $T \sim 300$ K. These results are qualitatively similar to the behavior observed in the non-superconducting spin-glass compositions, despite the fact that the positions of the incommensurate peaks change drastically across the insulator-superconductor boundary of the LSCO phase diagram. The behavior of this material $\text{La}_{1.93}\text{Sr}_{0.07}\text{CuO}_4$ is a crucial link in the chain of understanding how the static and dynamic spin correlations evolve from the insulator to the optimal superconductor.

V. ACKNOWLEDGMENTS

We would like to thank G. Shirane, K. Yamada, M. Matsuda, S. Wakimoto, K. Hirota, H. Kimura and M. A. Kastner for fruitful discussions. We also thank B. Keimer, M. Onodera, K. Nemoto, and L.P. Regnault for their assistance in our experiments. The present work was supported by the US-Japan Cooperative Research Program on Neutron Scattering, a Grant-in-Aid for Scientific Research of Monbusho, and the Core Research for Evolutional Science and Technology (CREST) Project

sponsored by the Japan Science and Technology Corporation. The work at MIT was supported by the U.S. National Science Foundation under contract numbers DMR-0071256 and DMR98-08941.

-
- ¹ M. A. Kastner, R. J. Birgeneau, G. Shirane and Y. Endoh, *Rev. Mod. Phys.*, **70**, 897 (1998).
 - ² S. M. Hayden, *Neutron Scattering in Layered Copper-Oxide Superconductors* (Kluwer Academic Publishers, Netherlands, 1998) ed. by A. Furrer, p.135.
 - ³ K. Yamada, C. H. Lee, K. Kurahashi, J. Wada, S. Wakimoto, S. Ueki, H. Kimura, Y. Endoh, S. Hosoya, G. Shirane, R. J. Birgeneau, M. Greven, M. A. Kastner and Y. J. Kim, *Phys. Rev. B*, **57**, 6165 (1998).
 - ⁴ K. Yamada, S. Wakimoto, G. Shirane, C. H. Lee, M. A. Kastner, S. Hosoya, M. Greven, Y. Endoh and R. J. Birgeneau, *Phys. Rev. Lett.*, **75**, 1626 (1995).
 - ⁵ C. H. Lee, K. Yamada, Y. Endoh, G. Shirane, R. J. Birgeneau, M. A. Kastner, M. Greven and Y. J. Kim, *J. Phys. Soc. Jpn.*, **69**, 1170 (2000).
 - ⁶ S. Wakimoto, R. J. Birgeneau, M. A. Kastner, Y. S. Lee, R. Erwin, P. M. Gehring, S. H. Lee, M. Fujita, K. Yamada, Y. Endoh, K. Hirota and G. Shirane, *Phys. Rev. B*, **61**, 3699 (2000).
 - ⁷ M. Matsuda, M. Fujita, K. Yamada, R. J. Birgeneau, M. A. Kastner, H. Hiraka, Y. Endoh, S. Wakimoto and G. Shirane, *Phys. Rev. B*, **62**, 9148 (2000).
 - ⁸ M. Fujita, K. Yamada, H. Hiraka, S. H. Lee, P. M. Gehring, S. Wakimoto and G. Shirane, cond-mat/0101320.
 - ⁹ H. Kimura, K. Hirota, H. Matsushita, K. Yamada, Y. Endoh, S. H. Lee, C. F. Majkrzak, R. Erwin, G. Shirane, M. Greven, Y. S. Lee, M. A. Kastner and R. J. Birgeneau, *Phys. Rev. B*, **59**, 6517 (1999).
 - ¹⁰ H. Matsushita, H. Kimura, M. Fujita, K. Yamada, K. Hirota and Y. Endoh, *J. Phys. Chem. Solid.*, **60**, 1071 (1999).
 - ¹¹ T. Suzuki, T. Goto, K. Chiba, T. Shinoda, T. Fukase, H. Kimura, K. Yamada, M. Ohashi and Y. Yamaguchi, *Phys. Rev. B*, **57**, R3229 (1998).
 - ¹² S. M. Hayden, G. Aeppli, R. Osborn, A. D. Taylor, T. G. Perring, S-W. Cheong and Z. Fisk, *Phys. Rev. Lett.*, **67**, 3622 (1991).
 - ¹³ S. Itoh, K. Yamada, M. Arai, Y. Endoh, Y. Hidaka and S. Hosoya, *J. Phys. Soc. Jpn.*, **63**, 4542 (1994).
 - ¹⁴ K. Yamada, Y. Endoh, C. H. Lee, S. Wakimoto, M. Arai, K. Ubukata, M. Fujita, S. Hosoya and S. M. Bennington, *J. Phys. Soc. Jpn.*, **64**, 2742 (1995).
 - ¹⁵ S. M. Hayden, G. Aeppli, H. A. Mook, T. G. Perring, T. E. Mason, S. W. Cheong and Z. Fisk, *Phys. Rev. Lett.*, **76**, 1344 (1996).
 - ¹⁶ B. Keimer, N. Belk, R. J. Birgeneau, A. Cassanho, C. Y. Chen, M. Greven, M. A. Kastner, A. Aharony, Y. Endoh, R. W. Erwin and G. Shirane, *Phys. Rev. B*, **46**, 14034 (1992).
 - ¹⁷ M. Matsuda, R. J. Birgeneau, Y. Endoh, Y. Hidaka, M. A. Kastner, K. Nakajima, G. Shirane, T. R. Thurston and K.

- Yamada, J. Phys. Soc. Jpn., **62**, 1702 (1993).
- ¹⁸ S. Hosoya, C. H. Lee, S. Wakimoto, K. Yamada and Y. Endoh, Physica C, **235-240**, 547 (1994).
 - ¹⁹ C. H. Lee, N. Kaneko, S. Hosoya, K. Kurahashi, S. Wakimoto, K. Yamada and Y. Endoh, Supercond. Sci. Technol., **11**, 891 (1998).
 - ²⁰ T. R. Thurston, P. M. Gehring, G. Shirane, R. J. Birgeneau, M. A. Kastner, Y. Endoh, M. Matsuda, K. Yamada, H. Kojima and I. Tanaka, Phys. Rev. B, **46**, 9128 (1992).
 - ²¹ M. Matsuda, K. Yamada, Y. Endoh, T. R. Thurston, G. Shirane, R. J. Birgeneau, M. A. Kastner, I. Tanaka and H. Kojima, Phys. Rev. B, **49**, 6958 (1994).
 - ²² M. J. Cooper and R. Nathans, Acta Cryst., **23**, 357 (1967).
 - ²³ G. Aeppli, T. E. Mason, S. M. Hayden, H. A. Mook and J. Kulda, Science, **278**, 1432 (1997).
 - ²⁴ M. Sato, S. Shamoto, T. Kiyokura, K. Kakurai, G. Shirane, B. J. Sternlieb and J. M. Tranquada, J. Phys. Soc. Jpn., **62**, 263 (1993).
 - ²⁵ S. Petit, A. H. Moudden, B. Hennion, A. Vietkin and A. Revcolevschi, Physica B, **234-236**, 800 (1997).
 - ²⁶ Y. Endoh, T. Fukuda, S. Wakimoto, M. Arai, K. Yamada and S. M. Bennington, J. Phys. Soc. Jpn., Suppl. B, **69**, 16 (2000).
 - ²⁷ A. Weidinger, Ch. Niedermayer, A. Golnik, R. Simon, E. Recknagel, J. I. Budnick, B. Chamberland and C. Baines, Phys. Rev. Lett., **62**, 102 (1989).
 - ²⁸ Ch. Niedermayer, C. Bernhard, T. Blasius, A. Golnick, A. Moodenbaugh and J. I. Budnick, Phys. Rev. Lett., **80**, 3843 (1998).